

# Eddy-current interaction with an ideal crack. I. The forward problem

J. R. Bowler

*The University of Surrey, Guildford, Surrey GU2 5XH, United Kingdom*

(Received 30 September 1993; accepted for publication 16 February 1994)

The impedance of an eddy-current probe changes when the current it induces in an electrical conductor is perturbed by a flaw such as a crack. In predicting the probe signals, it is expedient to introduce idealizations about the nature of the flaw. Eddy-current interaction is considered with an ideal crack having a negligible opening and acting as an impenetrable barrier to electric current. The barrier gives rise to a discontinuity in the electromagnetic field that has been calculated by finding an equivalent electrical source distribution that produces the same effect. The choice of source is between a current dipole layer or a magnetic dipole layer; either will give the required jump in the electric field at the crack. Here a current dipole layer is used. The strength of the equivalent source distribution has been found by solving a boundary integral equation with a singular kernel. From the solution, the probe impedance due to the crack has been evaluated. Although analytical solutions are possible for special cases, numerical approximations are needed for cracks of arbitrary shape. Following a moment method scheme, numerical predictions have been made for both rectangular and semielliptical ideal cracks. These predictions have been compared with experiments performed on narrow slots used to simulate ideal cracks. Good agreement has been found between the calculations and the measurements.

## I. THEORETICAL APPROACH

In eddy-current nondestructive evaluation, a flaw is usually detected from the observation of probe impedance changes due to the interaction between induced oscillating electrical current in a conductor and the defect. Theoretically, the interaction may be treated as a scattering problem in which the scattered field is determined from a knowledge of the incident field and the nature of the flaw. The solution must take account of the shape and material properties of both the flaw and the conductor, ensuring that the electromagnetic field satisfies the correct continuity and boundary conditions.

In tackling the problem using an integral equation technique, the scattered field may be expressed as either a volume<sup>1,2</sup> or a surface integral.<sup>3</sup> In either case, an integral equation can be derived containing a kernel that embodies the boundary conditions of the unflawed conductor. In this way, these boundary conditions are satisfied for an arbitrary flaw. The approach works best for simple conductors such as a homogeneous half-space,<sup>4</sup> an infinite cylinder,<sup>5</sup> or multilayered planar structures,<sup>6</sup> since explicit Green's kernels are known in such cases and are relatively easy to evaluate numerically. With a known Green's function, the essence of the scattering problem is to determine the electromagnetic field in a flaw region or, by considering the flaw as a secondary source, determine its effective source strength.

A small flaw in a nonmagnetic conductor, such as a small spherical cavity, disturbs the induced current and produces the same perturbed field as a current dipole, the dipole strength being proportional to the incident field at the flaw site.<sup>7</sup> More generally, the equivalent source of the perturbed field due to a volumetric flaw, such as a finite cavity, can be expressed as a three-dimensional current dipole distribution.<sup>1</sup> A Fredholm integral equation of the second kind has been used to determine the effective dipole density in the flaw

volume and approximate solutions of this equation computed using the moment method.<sup>8</sup> Predictions of the impedance due to the flaw may be found using an equation derived from a reciprocal relationship.<sup>1</sup>

It is possible to predict the probe response due to a crack by treating it as a thin volumetric flaw but a more elegant and efficient alternative is to consider eddy-current interaction with an ideal crack. An ideal crack is defined as a flaw of zero thickness acting as an impenetrable surface barrier to electric current. In discussing a two-dimensional version of this problem, Kahn, Spal, and Feldman<sup>9</sup> adapted Sommerfeld's solution for the diffraction of a wave at a semi-infinite half-plane<sup>10</sup> to determine the field in the region of the crack edge. A different ideal crack problem, involving a through crack in a thin plate, has been solved by Burke and Rose<sup>11</sup> for the case where the plate thickness is small in comparison with the skin depth. In spite of the restriction on the skin depth, the thin plate solution agrees with experiment over a wide frequency range.

The present study is a two-part examination of the general ideal crack problem using a boundary integral formulation valid for an arbitrary skin depth.<sup>12</sup> In this, the first part, the forward problem is formulated and approximate numerical solutions found using boundary elements. The use of a rapid numerical procedure for finding approximate solutions paves the way for part II which considers the inverse problem. In ideal crack inversion, the aim is to estimate the shape of an unknown crack from a finite number of probe impedances. In the inversion scheme proposed, the flaw is modified iteratively until the forward problem gives optimum predictions which match the data as closely as possible in a least-squares sense. For a successful least-squares inversion scheme, the forward calculation described here in part I has been developed to be flexible enough to cope with any flaw shape that will be encountered and sufficiently fast so that the inversion does not take an inordinate amount of time.

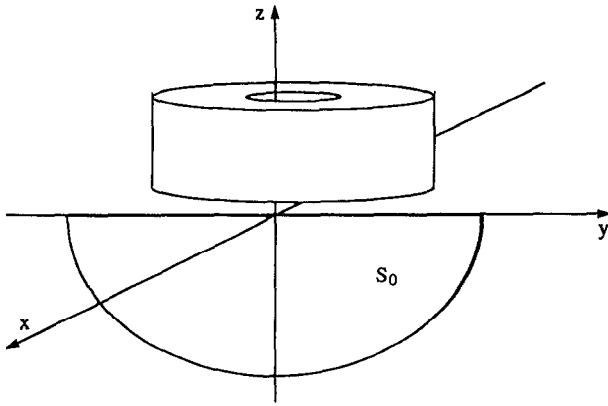


FIG. 1. Ideal crack and a normal excitation coil.

We begin the account of the forward problem by considering the crack boundary conditions. This is followed by a description of the integral formulation and details of the numerical scheme. Comparisons of predictions with experimental measurements on narrow slots produced by electric discharge machining are reported, and finally the conclusions are stated.

## II. SECONDARY SOURCE

Boundary integral methods for solving electromagnetic problems are usually based on one of the variants of Green's second theorem. Application of a vector version of the theorem leads us to consider the tangential components of the electric and magnetic fields on a suitable regular closed surface.<sup>5</sup> An ideal crack is defined on an open surface  $S_0$ , say (Fig. 1), but by collapsing the closed surface onto the crack (Fig. 2) it is possible to derive an integral equation for the surface field on  $S_0$ . In anticipation of this derivation, we consider first the boundary conditions at the crack.

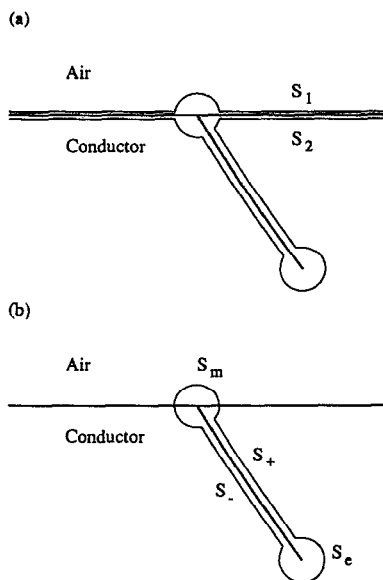


FIG. 2. (a) Surfaces  $S_1$  and  $S_2$ ; (b) surface  $S$  enclosing the crack.

At an interface between dissimilar materials, the tangential magnetic field is continuous. One of the standard textbook arguments to justify this statement is to invoke Ampere's circuital law, applying it to a small rectangular loop whose shortest sides cross the interface.<sup>13</sup> In the limit as the shortest sides vanish the only contribution to the line integral of the magnetic field around the circuit comes from the longer sides of the rectangle. If there are no singular surface currents tangential to the interface, the net current through the loop is zero in the limit, therefore the two remaining contributions to the line integral from the longer sides of the rectangle sum to zero. For this sum to be zero for all possible rectangles, the tangential magnetic field must be the same on either side of the interface. Without modification the same argument applies at the crack surface  $S_0$  and the tangential magnetic field satisfies the continuity condition

$$\mathbf{H}_t^+ - \mathbf{H}_t^- = \Delta \mathbf{H}_t = 0, \quad (1)$$

where the  $\pm$  signs refer to limiting values approaching each side of  $S_0$  and the subscript  $t$  denotes tangential components.

From the fact that the net magnetic flux through an arbitrary closed surface is zero, it can be shown using another well-known argument<sup>4</sup> that the normal flux is continuous at  $S_0$ , a condition that is expressed as

$$B_n^+ - B_n^- = \Delta B_n = 0, \quad (2)$$

where the subscript  $n$  denotes a normal component.

The current density is, in general, discontinuous at an ideal crack and therefore the same must be true of the electric field. It follows from Eq. (2) and Faraday's induction law that the discontinuity in the tangential electric field  $\Delta \mathbf{E}_t$  satisfies the condition  $\hat{n} \cdot \nabla \times \Delta \mathbf{E}_t = \nabla \cdot (\hat{n} \times \Delta \mathbf{E}_t) = 0$ , which means that the jump in the electric field at the crack may be expressed as the gradient of a surface scalar function. Thus,

$$\mathbf{E}_t^+ - \mathbf{E}_t^- = \Delta \mathbf{E}_t = -\frac{1}{\sigma} \nabla_t p, \quad (3)$$

where  $\sigma$  is the conductivity of the material,  $p$  is a surface scalar function defined on  $S_0$ , and  $\nabla_t$  is the tangential gradient. A similar equation for the jump in the tangential electric field at a surface arises in electrostatics but in electrostatic theory the dielectric permittivity is written in place of the conductivity and the surface is populated by charge dipoles.<sup>15</sup> In eddy-current theory the analogous argument leading to Eq. (3) involves a source layer of current dipoles orientated normal to the surface. Equation (3) defines  $p$  apart from a constant that disappears when the gradient is taken. The constant is chosen such that  $p$  vanishes at the crack edge, a condition necessary for ensuring that the energy of the dipole distribution is finite. With  $\hat{n}$  the unit vector normal to  $S_0$ , the current dipole distribution  $\mathbf{p} = \hat{n} p$  represents the electric source equivalent of an ideal crack.

An alternative equivalent source is a layer of oscillating magnetic dipoles whose surface density  $\mathbf{m}$  is related to the jump in the electric field at  $S_0$  by  $\hat{n} \times \Delta \mathbf{E}_t = i\omega\mu_0\mathbf{m}$ .<sup>14</sup> The magnetic dipoles are orientated in the direction tangential to the crack surface and normal to the direction of the jump in the electric field. The implicit time dependence is of the form  $\exp(-i\omega t)$ . In the thin plate problem of Burke and Rose,<sup>11</sup>

the vortices invoked to represent the equivalent source of an ideal crack are, by another name, magnetic dipoles.

For numerical calculations, the electric current dipole distribution has an advantage in that it is a single component vector and therefore requires fewer unknowns. Also, the current dipole density remains finite at the crack edge whereas the magnetic dipole density tends to infinity as the edge is approached. Although not an insurmountable problem, the edge infinity in the magnetic source can be an inconvenience in numerical calculations.

An ideal crack, by definition, allows no current to pass across it, which means that the normal component of the current at  $S_0$  is zero. Although the crack surface will carry an oscillating charge, the charging current is of the order of the displacement current across the crack and is, therefore, negligible in most cases of practical interest. The condition on the normal current, written as

$$J_n^\pm = 0, \quad (4)$$

will be used together with an integral equation for the field to determine the dipole density  $p$ .

For ferromagnetic materials, the above boundary conditions are valid but are not necessarily appropriate because the finite opening of a real defect in a high-permeability material has a significant effect on the field adjacent to the crack faces. It may be necessary to use a different idealization for modeling cracks in, say, ferrous steel, but for materials that are not ferromagnetic, the boundary conditions specified by Eqs. (1)–(4) approximate the field adjacent to a crack or slot of narrow opening.

### III. DIPOLE DENSITY

The integral equation for the dipole density at an ideal crack in an otherwise homogeneous conductor may be derived starting with the differential equation for the electric field. Excluding the flawed region, the perturbed electric field  $\mathbf{E}_j$ , satisfies

$$\nabla \times \nabla \times \mathbf{E}_j(\mathbf{r}) - k_j^2 \mathbf{E}_j(\mathbf{r}) = 0, \quad (5)$$

where subscript  $j$  refers to the nonconducting ( $j=1$ ,  $k_1=0$ ) and conducting ( $j=2$ ,  $k_2^2=k^2=i\omega\mu_0\sigma$ ) regions. To get an integral solution of Eq. (5), the electric dyadic Green's functions  $\mathcal{G}_j(\mathbf{r}|\mathbf{r}')$ ,  $j=1,2$  are introduced satisfying

$$\nabla \times \nabla \times \mathcal{G}_j(\mathbf{r}|\mathbf{r}') - k_j^2 \mathcal{G}_j(\mathbf{r}|\mathbf{r}') = \delta(\mathbf{r}-\mathbf{r}')\mathcal{I}, \quad (6)$$

where  $\mathcal{I}$  is the unit tensor and  $\mathbf{r}'$  is the coordinate of a source point in the conductor.  $\mathcal{G}_1$  and  $\mathcal{G}_2$  are considered as electric dyadic Green's functions because they satisfy the same continuity and boundary conditions as the electric field, namely,

$$\hat{\mathbf{e}} \times \mathcal{G}_1 = \hat{\mathbf{e}} \times \mathcal{G}_2, \quad \frac{1}{\mu_1} \hat{\mathbf{e}} \times \nabla \times \mathcal{G}_1 = \frac{1}{\mu_2} \hat{\mathbf{e}} \times \nabla \times \mathcal{G}_2,$$

and

$$\lim_{|\mathbf{r}'| \rightarrow \infty} \mathcal{G}_j = 0, \quad (7)$$

where  $\hat{\mathbf{e}}$  is a unit vector normal to the interface. The first of these conditions ensures that the tangential components of

the electric field are continuous at the surface of the conductor, the second ensures a continuous tangential magnetic field, and the third condition guarantees that the solution vanishes as  $|\mathbf{r}'| \rightarrow \infty$ .

An equation for the current dipole density may be found that is valid for surface breaking and subsurface cracks. In the argument presented below, it is necessary to consider the singular behavior of the field at the periphery of the defect, both at the buried edge and where the crack intersects the surface. The nature of the edge singularities is significant in transforming the integral relationship that is found from Green's second theorem. It is not necessary to have a complete solution of the problem to establish the form that these field singularities take; all that is needed is an idea of the local solution on a scale that is small compared with the skin depth and the radius of curvature of the crack edge. On such a small scale the form of the edge singularities can be established from approximate local fields satisfying the Laplace equation. The aim has been to derive an integral equation involving the crack surface  $S_0$  and avoid the possibility of having to include a line integral to represent edge effects.

Using Eqs. (5) and (6) and a regular surface  $S$  enclosing the defect, Green's theorem in the form

$$\begin{aligned} & \int_V (\mathbf{C} \cdot \nabla \times \nabla \times \mathbf{A} - \mathbf{A} \cdot \nabla \times \nabla \times \mathbf{C}) d\mathbf{r} \\ &= \int_S [(\mathbf{A} \times \nabla \times \mathbf{C}) - \mathbf{C} \times \nabla \times \mathbf{A}] \cdot d\mathbf{S} \end{aligned} \quad (8)$$

may be invoked to show that<sup>5</sup>

$$\begin{aligned} \mathbf{E}(\mathbf{r}) = & \mathbf{E}^{(0)}(\mathbf{r}) - \int_S \{[\hat{\mathbf{n}} \times \mathbf{E}(\mathbf{r}')] \cdot \nabla' \times \mathcal{G}(\mathbf{r}'|\mathbf{r}) \\ & + i\omega\mu_0[\hat{\mathbf{n}} \times \mathbf{H}(\mathbf{r}')] \cdot \mathcal{G}(\mathbf{r}'|\mathbf{r})\} dS', \end{aligned} \quad (9)$$

where  $\hat{\mathbf{n}}$  is an outwardly directed unit vector normal to  $S$  and  $\mathbf{E}^{(0)}(\mathbf{r})$  is the unperturbed electric field. The subscript  $j=1,2$  has been dropped. Equation (9) is derived by applying Green's theorem to the two surfaces  $S_1$  and  $S_2$  [Fig. 2(a)]. The resulting equations are added, the two surfaces brought together at the interface, and the interface continuity conditions used to reduce the surface of integration to  $S$ .

The regular surface  $S$  consists of  $S_+$  and  $S_-$  adjacent to the crack faces, a surface  $S_e$  encircling the buried edge and a surface  $S_m$  encircling the crack mouth [Fig. 2(b)]. Allow  $S$  to collapse onto the open surface  $S_0$  and consider the way Eq. (9) is modified in the process. In the limit, Eqs. (1) and (3) can be used to simplify the integral over the faces. Examine first, however, the behavior of the integral over  $S_e$  as the radius of  $S_e$  vanishes.

At a buried edge, the integral over  $S_e$  involves a weak singularity<sup>9</sup> at which the magnetic field is finite but the electric field varies in magnitude as  $\rho^{-1/2}$ ,  $\rho$  being the perpendicular distance from a point to the crack edge. For small  $\rho$ , the integral over  $S_e$  is of the order  $\rho^{1/2}$  and therefore vanishes with  $\rho$  for any field point not at the crack edge.

Although the buried edge integral vanishes, the field in air near the crack mouth involves components of the order  $1/\rho$ . In spite of the presence of such terms, it is possible to

obtain an equation for the dipole density that does not involve edge integrals. This conclusion is reached by considering the nature of the electromagnetic field close to the line where the crack meets the surface of the conductor.

Near the crack mouth, local Laplacian corner solutions describe the electromagnetic field in the conductor. It is evident from the corner solutions inside the conductor that both the electric and the magnetic fields are finite in this region. Therefore, the corner contribution to the integral over  $S_m$  will vanish in the limit as the enclosing surface collapses. Outside the conductor, the field in the vicinity of the mouth of an ideal crack is singular. In characterizing the external field, we refer to the intersection of the crack surface with the surface of the conductor as the line of the crack. Local solutions given below describe separately components of the electric field perpendicular to the line of the crack and parallel to this line. Although these field components are coupled and the solution in this region is complicated, the essential behavior is exhibited by the approximate local solutions of Eq. (5). Apart from a smoothly varying background that does not concern us at present, the external electric field in the direction of the line of the crack is approximated by

$$\mathbf{E}_U = \frac{\Delta E_t \phi}{\pi} \hat{u}, \quad (10)$$

where  $\hat{u}$  is a unit vector in the direction of the crack line and  $\phi$  is an azimuthal angle measured in the plane perpendicular to  $\hat{u}$  from the direction of the normal to the surface of the conductor ( $-\pi/2 \leq \phi \leq \pi/2$ ). The term  $\Delta E_t$  is the jump in the electric field across the crack mouth. Equation (10) applies on a scale that is small compared with both the crack size and skin depth. It gives the local field associated with the current contraflow divided at the line of intersection of the surface of the conductor and the crack. It may be verified that Eq. (10) satisfies Eq. (5) (with  $j=1, k_1=0$ ) on a small scale where  $\Delta E_t$  is locally constant. From the induction law, the corresponding magnetic field is

$$i\omega\mu_0\mathbf{H}_U = \nabla \times \mathbf{E}_U = -\frac{\Delta E_0}{\pi\rho} \hat{u}_\rho, \quad (11)$$

where  $\hat{u}_\rho$  is a radial unit vector. Here the singular behavior of the magnetic field is exhibited in the radial component and not in the components tangential to the surface  $S_m$ . Therefore the corresponding integral over  $S_m$  vanishes in the limit as the radius of  $S_m$  goes to zero.

An additional contribution to the electric field arises due to the potential drop across the crack mouth. Using  $\hat{\phi}$  to denote an azimuthal unit vector defined with respect to the direction of the crack edge, the potential has the local form

$$V = \frac{\Delta V}{\pi} \phi, \quad (12)$$

where  $\Delta V$  is the potential drop across the crack. The corresponding electric field is

$$\mathbf{E}_V = -\nabla V = -\frac{\Delta V}{\pi} \frac{1}{\rho} \hat{\phi}, \quad (13)$$

where, once again,  $\rho$  is the cylindrical polar radial coordinate defined with respect to the line of the crack. Equation (13) contains a  $1/\rho$  singularity that will give rise to a nonvanishing contribution to the integral over  $S_m$  in the limit as the radius of  $S_m$  goes to zero.

In summary, we have established, from the continuity condition, Eq. (1), and the nature of the field at the perimeter of the ideal crack, that the magnetic-field term in Eq. (9) does not contribute to the scattered electric field in the limit as  $S$  collapses onto  $S_0$ . Furthermore, Eqs. (3) and (13) show that only the conservative part of the electric field contributes in the limit and it does so both through a contribution from the mouth and through an integral over the crack faces. In the subsequent development, a transformation is made to absorb the mouth contribution into a surface integral over  $S_0$ .

In general, the tangential electric field on the surface  $S$  can be expressed in terms of two scalar functions as  $\mathbf{E}_t(\mathbf{r}) = -\nabla_t V(\mathbf{r}) + \nabla \times [\hat{n}U(\mathbf{r})]$  but in the limit as  $S$  collapses onto  $S_0$ , continuous and finite parts of the field will not contribute to the resulting integral. Hence, the contribution arising from  $\nabla \times [\hat{n}U(\mathbf{r})]$  vanishes in the limit. This means we need only consider a surface integral involving the part of the tangential electric field that is contained in the term  $-\nabla_t V(\mathbf{r})$ . Note that the continuity of the tangential electric field implies that the potential  $V(\mathbf{r})$  is continuous at the air-conductor interface. From the jump in the electric field at the crack one can identify  $\Delta V(\mathbf{r}) = p(\mathbf{r})/\sigma$ . The nonvanishing part of the integral from Eq. (9) is transformed as follows:

$$\begin{aligned} & \int_S [\hat{n} \times \nabla V(\mathbf{r}')] \cdot \nabla \times \mathcal{G}(\mathbf{r}'|\mathbf{r}) dS' \\ &= \int_S \hat{n} \{ \nabla \times [V(\mathbf{r}') \nabla \times \mathcal{G}(\mathbf{r}'|\mathbf{r})] \\ & \quad - V(\mathbf{r}') \nabla \times \nabla \times \mathcal{G}(\mathbf{r}'|\mathbf{r}) \} dS'. \end{aligned} \quad (14)$$

Applying the Stokes theorem to the first term on the right-hand side shows that its contribution vanishes since  $S$  is a closed surface. Hence, in the limit as  $S_+$  and  $S_-$  approach the crack faces,

$$\begin{aligned} \mathbf{E}(\mathbf{r}) &= \mathbf{E}^{(0)}(\mathbf{r}) - \int_{S_0} \hat{n} \cdot [\Delta V(\mathbf{r}) \nabla' \times \nabla' \times \mathcal{G}(\mathbf{r}'|\mathbf{r})] dS' \\ &= \mathbf{E}^{(0)}(\mathbf{r}) + i\omega\mu_0 \int_{S_0} \mathcal{G}(\mathbf{r}|\mathbf{r}') \cdot \mathbf{p}(\mathbf{r}') dS'. \end{aligned} \quad (15)$$

Here the integrand is transformed using Eq. (6), we use the fact that  $\Delta V(\mathbf{r}) = p(\mathbf{r})/\sigma$  and apply the symmetry relationship<sup>5</sup>  $\mathcal{G}(\mathbf{r}|\mathbf{r}') = \mathcal{G}^T(\mathbf{r}'|\mathbf{r})$ , where  $T$  denotes the transpose of the dyad.

Multiplying Eq. (15) by the conductivity  $\sigma$  and applying the condition, Eq. (4), that the normal component of the current density at the crack surface is zero, gives

$$J_n^{(0)}(\mathbf{r}_\pm) = -k^2 \lim_{\mathbf{r} \rightarrow \mathbf{r}_\pm} \int_{S_0} G^{nn}(\mathbf{r}|\mathbf{r}') p(\mathbf{r}') dS', \quad (16)$$

where  $J_n^{(0)}(\mathbf{r}_\pm) = \sigma \hat{n} \cdot \mathbf{E}^{(0)}(\mathbf{r}_\pm)$  and  $G^{nn}(\mathbf{r}|\mathbf{r}') = \hat{n} \cdot \mathcal{G}(\mathbf{r}|\mathbf{r}') \cdot \hat{n}$ . Equation (16) determines the current dipole density on the surface  $S_0$ .

The nature of the singularity in the Green's function means that Eq. (16) involves an improper integral that is interpreted in the limit by Hadamard's theory of the finite part.<sup>16,17</sup> Unfortunately this interpretation is not helpful for numerical boundary element calculations. To calculate the singular matrix element, the region of integration is separated into two parts: a finite exclusion zone  $S_\epsilon$  adjacent to the field point, and a region remote from the field point that can be treated using a standard numerical quadrature scheme. Here the integral over  $S_\epsilon$  is evaluated analytically with a near-field approximation of the kernel, then the limit is taken as the field point approaches the center of the exclusion zone. The details of this procedure are given in Sec. VI following a discussion of the dyadic kernel.

#### IV. GREEN'S DYAD

The quasistatic dyadic Green's function for an electric source in a half-space conductor satisfying Eq. (6) and the boundary conditions (7) was derived by Raiche and Coggon.<sup>4</sup> Closely related earlier work on dipoles in a half-space is reviewed in the text by Banos.<sup>18</sup> Using an analysis based on a scalar decomposition of the field using Hertz potentials,<sup>19</sup> the half-space dyadic Green's function giving the electric field due to an electric source can be written as

$$\mathcal{G}(\mathbf{r}|\mathbf{r}') = \left( \mathcal{I} + \frac{1}{k^2} \nabla \nabla \right) \cdot [\mathcal{I} \phi(\mathbf{r}|\mathbf{r}') + \mathcal{I}' \phi(\mathbf{r}|\mathbf{r}' - 2\hat{z}z')] + \frac{1}{k^2} \{ \nabla \times \hat{z} [\nabla' \times \hat{z} V(\mathbf{r}|\mathbf{r}')] \}, \quad (17)$$

where  $\mathcal{I} = \hat{x}\hat{x} + \hat{y}\hat{y} - \hat{z}\hat{z}$  is a modified unit dyad that reverses the sign of the  $z$  component of a vector,

$$\phi(\mathbf{r}|\mathbf{r}') = \frac{e^{ik|\mathbf{r}-\mathbf{r}'|}}{4\pi|\mathbf{r}-\mathbf{r}'|} \quad (18)$$

and

$$V(\mathbf{r}|\mathbf{r}') = \pm \frac{1}{2\pi} L_z(k, \rho, |z+z'|) - 2\phi(\mathbf{r}|\mathbf{r}' - 2\hat{z}z'), \quad (19)$$

where  $\rho^2 = (x-x')^2 + (y-y')^2$ . Here the  $+$  sign holds if  $z+z' < 0$  and the  $-$  sign if  $z+z' > 0$ . Equation (19) contains the function  $L_z = \partial L / \partial z$  where  $L$  is given by the Foster-Lien integral,<sup>18</sup>

$$L(k, \rho, \zeta) = \int_0^\infty \frac{1}{\gamma} e^{-\gamma \zeta} J_0(\rho s) ds = I_0[-ik(S-\zeta)/2] K_0[-ik(S+\zeta)/2], \quad (20)$$

where  $S^2 = \rho^2 + \zeta^2$  and  $\gamma = \sqrt{S^2 - k^2}$ , taking the root with a positive real part. Here we have taken  $\sqrt{-k^2} = -ik$  since the integral requires that this parameter has a positive real part.<sup>20</sup>

Equation (17) contains the unbounded domain dyadic Green's function, an image term and a transverse electric term,  $(1/k^2) \nabla \times \hat{z} [\nabla' \times \hat{z} V(\mathbf{r}|\mathbf{r}')]$  accounting for the fact the reflection from the interface is partial. The differentiation of the transverse electric potential is presented in the Appendix

where the results are given in terms of Kelvin functions. For the numerical calculations, the Kelvin functions are approximated by polynomials.<sup>21</sup>

#### V. IMPEDANCE

The eddy-current probe impedance change due to an ideal crack is given in terms of the coil current  $\mathbf{J}(\mathbf{r})$  and the scattered electric field  $\mathbf{E}^{(s)}(\mathbf{r})$  by

$$I^2 \Delta Z = - \int_{\text{coil}} \mathbf{E}^{(s)}(\mathbf{r}) \cdot \mathbf{J}(\mathbf{r}) d\mathbf{r}, \quad (21)$$

where the integral is over the coil region. The scattered electric field  $\mathbf{E}^{(s)}(\mathbf{r})$  is given by the integral of Eq. (15). An alternative and more convenient expression for the impedance is found from Eq. (21) using a reciprocity principle<sup>22</sup> based on the vector Green's theorem, Eq. (8), with  $\mathbf{C} = -\mathbf{E}^{(s)}$  and  $\mathbf{A} = \mathbf{E}^{(0)}$ . Using the field equation (5) with the source term  $\mathbf{J}(\mathbf{r})$  included, the impedance is expressed as a surface integral. The choice of the surface is somewhat arbitrary, but initially the surface  $S$  defined earlier and illustrated in Fig. 2(a) is chosen, allowing  $S$  to collapse onto  $S_0$  as before to give the desired result,

$$I^2 \Delta Z = - \int_{S_0} \mathbf{E}^{(0)}(\mathbf{r}) \cdot \mathbf{p}(\mathbf{r}) dS. \quad (22)$$

The application of the reciprocity relationship is slightly complicated by the fact that the primary and secondary sources are in different regions, but this is taken into account by starting with two surfaces as shown in Fig. 2(a), combining these to form  $S$  while making use of the field continuity conditions that apply at the air-conductor interface.

The unperturbed electric field in the conductor due to a coil with an axis of symmetry normal to the interface is given by

$$\mathbf{E}^{(0)}(\rho, z) = i\omega\mu_0 I \hat{\phi} \int_0^\infty \frac{\kappa}{\gamma_0 + \kappa} e^{\gamma_0 z} S(\kappa) J_1(\kappa\rho) d\kappa, \quad (23)$$

where  $\gamma_0 = \sqrt{\kappa^2 - i\omega\mu_0\sigma}$ , taking the root with a positive real part. The coil function  $S(\kappa)$ , is a combined Laplace and Hankel transform of the coil turns density  $n(\rho, z)$  and is given by

$$S(\kappa) = \int_0^\infty \int_0^\infty n(\rho, z) \exp(-\kappa z) J_1(\kappa\rho) \rho d\rho dz. \quad (24)$$

In the case of a coil with a rectangular cross section and a uniform turns density  $n_0$ , the turns density function is given by

$$n(\rho, z) = \begin{cases} n_0 & \text{if } a_2 < \rho < a_1, \text{ and } -b < z - h < b, \\ 0 & \text{otherwise,} \end{cases} \quad (25)$$

where  $a_1$  is the outer radius of the coil and  $a_2$  the inner radius.  $2b$  is the axial length and  $h$  the height of the coil center above the surface of the conductor. Integrating Eq. (24) with the turns density constant gives

$$S(\kappa) = \frac{2n_0}{\kappa} \exp(-\kappa h) \sinh(b\kappa) [a_1^2 \chi(a_1\kappa) - a_2^2 \chi(a_2\kappa)], \quad (26)$$

where  $\chi$  arises from the radial integration in Eq. (24) and is defined in terms of a standard integral by<sup>23</sup>

$$\chi(\alpha) = \int_0^{-1} J_1(\alpha\rho)\rho d\rho = \frac{\pi}{2\alpha} [J_1(\alpha)\mathbf{H}_0(\alpha) - J_0(\alpha)\mathbf{H}_1(\alpha)], \quad (27)$$

$\mathbf{H}_0$  and  $\mathbf{H}_1$  being Struve functions.

## VI. NUMERICAL SOLUTION

A discrete approximation of Eq. (16) has been found for plane ideal cracks of arbitrary shape perpendicular to the surface of the conductor. The coordinate system has been chosen such that the crack is in the plane  $x=0$  (Fig. 1). For the numerical calculations, it is convenient to work with a rectangular domain  $S_r$  rather than the domain of the crack  $S_0$ . Introducing a characteristic function  $\gamma(y,z)$  into the integrand of Eq. (16) allows an extension of the domain of integration. By definition, the characteristic function is 1.0 at any point on the crack surface and zero elsewhere in the crack plane. With the extended domain  $S_r$ , Eq. (16) can be written in the modified form

$$J_n^{(0)}(\mathbf{r}_\pm) = -k^2 \lim_{\mathbf{r} \rightarrow \mathbf{r}_\pm} \int_{S_r} G^{xx}(\mathbf{r}|\mathbf{r}') \gamma(\mathbf{r}') p(\mathbf{r}') dS', \quad (28)$$

where  $G^{xx}(\mathbf{r}|\mathbf{r}') = \hat{x} \cdot \mathcal{G}(\mathbf{r}|\mathbf{r}') \cdot \hat{x}$ . A discrete approximation of Eq. (28) is formed by expanding the characteristic function and the dipole density in terms of pulse functions. The pulse functions are defined on a rectangular lattice filling the region  $S_r$  with cells whose dimensions are  $\delta_y \times \delta_z$ . Thus,

$$\gamma(y,z) \approx \sum_{l,m} \gamma_{lm} P_l \left( \frac{y}{\delta_y} \right) P_m \left( \frac{z}{\delta_z} \right)$$

and

$$p(y,z) \approx \sum_{l,m} p_{lm} P_l \left( \frac{y}{\delta_y} \right) P_m \left( \frac{z}{\delta_z} \right), \quad (29)$$

where the summations are over all cells and

$$P_j(u) = \begin{cases} 1.0 & \text{if } -\frac{1}{2} \leq u - j < \frac{1}{2}, \\ 0 & \text{otherwise.} \end{cases} \quad (30)$$

The coefficients  $\gamma_{lm}$  are predefined as 1.0, zero, or some intermediate value depending on whether a particular rectangular cell is inside, outside, or on the border of the crack. The optimum choice is given by

$$\gamma_{lm} = \int_{S_{lm}} \gamma(\mathbf{r}) dS, \quad (31)$$

where  $S_{lm}$  is the domain of the  $lm$  cell. Substituting Eq. (29) into Eq. (28) and demanding that the resulting equation is satisfied only at the central point of each rectangle,  $\mathbf{r}_{lm}$ , the piecewise constant dipole density is given by

$$\bar{\mathbf{J}} = (\bar{\gamma} \bar{\mathbf{G}} \bar{\gamma}) \bar{\mathbf{p}}, \quad (32)$$

where the elements of the vector  $\bar{\mathbf{J}}$  are  $J_{lm} = \delta J_n^{(0)}(\mathbf{r}_{lm}) \gamma_{lm}$ , and the matrix  $\bar{\gamma}$  is diagonal with  $\gamma_{lm}$  as its diagonal elements. The matrix elements of  $\bar{\mathbf{G}}$  are given by

$$G_{lm,LM} = \delta k^2 \int_{S_{LM}} G^{xx}(\mathbf{r}_{lm}|\mathbf{r}') dS'. \quad (33)$$

The skin depth  $\delta$ , used as a scaling factor, ensures that the matrix elements are dimensionless.

The solution of Eq. (32), giving the piecewise constant approximation of the dipole density, is found by carrying out a LU decomposition of the matrix  $\bar{\mathbf{G}}$ . Because  $\bar{\gamma}$  is diagonal, the LU decomposition is retained in forming the matrix product  $\bar{\gamma} \bar{\mathbf{G}} \bar{\gamma}$ . The solution is then found by backsubstitution. A major advantage of the scheme, particularly for inversion, is that the decomposition is done on a flaw-independent matrix. This means that it is only necessary to decompose once for any number of flaws defined on the same grid.

The crack impedance in discrete form is given by

$$I^2 \Delta Z \approx \frac{\delta_y \delta_z}{\delta \sigma} \sum_{l,m} J_{lm} p_{lm}. \quad (34)$$

This follows from Eqs. (22) and (29) plus the approximation that the value of  $E_n^{(0)}$  averaged over a cell is equal to the value at the center.

The matrix elements of  $\bar{\mathbf{G}}$ , expressed as the sum of a free-space and a reflection term, are of the form

$$G_{lm,LM} = G_{|l-L|,|m-M|}^{(0)} + G_{|l-L|,m+M}^{(\Gamma)}. \quad (35)$$

Using Eq. (17), these separate contributions are given by

$$G_{lm}^{(0)} = \delta \int_{S_{lm}} \left( k^2 + \frac{\partial^2}{\partial x^2} \right) \phi(\mathbf{0}|\mathbf{r}) dS, \quad \{l,m\} \neq \{0,0\} \quad (36)$$

and

$$G_{lm}^{(\Gamma)} = G_{lm}^{(0)} - \delta \int_{S_{lm}} \frac{\partial^2 V(\mathbf{0}|\mathbf{r})}{\partial y^2} dS. \quad (37)$$

All but the singular matrix element are calculated from Eqs. (36) and (37) using a numerical quadrature scheme. Evaluation of the singular element is carried out by subdividing the region of integration into a square exclusion zone of side  $2a$ , and a region outside the square covering the remainder of the singular cell. The integral over the exclusion zone is given by

$$I_{00} = 4 \delta \lim_{x \rightarrow 0} \left[ \int_0^a \int_0^a \left( k^2 + \frac{\partial^2}{\partial x^2} \right) \phi(R) dy dz \right], \quad (38)$$

where  $\phi(R) = e^{ikR}/(4\pi R)$  and  $R^2 = x^2 + y^2 + z^2$ . By expanding  $\phi(R)$  as a power series in  $ikR$ , integrating term by term and taking the limit,  $I_{00}$  is expressed as a power series expansion in  $ika$ . If we ensure that the size of a cell is much smaller than a skin depth, a reasonable approximation is obtained by terminating the series after a few terms. Terminating at fifth order, the integral of the free-space Green's function over the exclusion region is given by

$$I_{00} \approx \frac{\delta}{\pi a} \sum_{\nu=0,5} c_\nu (ika)^\nu, \quad (39)$$

where

$$c_\nu = \frac{\nu-1}{\nu!} \lim_{x \rightarrow 0} \int_0^1 \int_0^1 R^{\nu-3} \left( (\nu-3) \frac{x^2}{R^2} - (\nu-1) \right) dy dz. \quad (40)$$

Evaluating the coefficients gives

$$c_0 = \sqrt{2}, \quad c_1 = 0, \quad c_2 = -\ln(1 + \sqrt{2}),$$

$$c_3 = -\frac{2}{3}, \quad c_4 = -\frac{1}{8}[\sqrt{2} + \ln(1 + \sqrt{2})], \quad c_5 = -\frac{4}{45}.$$

Adding  $I_{00}$  to the result of the integration over the region of the singular cell outside the exclusion zone gives the value of the singular matrix element. This value should be independent of the size of the exclusion region. However, numerical errors are introduced first by terminating the series (39) and second in the numerical quadrature used to integrate outside the exclusion zone. A good test of the scheme is to vary  $a$  and examine any changes that might occur in the value of the singular matrix element. Although it is not possible to state precisely how small these changes should be, it is prudent to ensure that they are much smaller than the overall error in the impedance predictions.

The nature of the singularity means that the leading term in  $I_{00}$  is of the order  $1/a$ . This dependence is a feature of the singular matrix element found by integrating the dyadic Green's function over a surface.<sup>24,25</sup> In the singular element calculation the contribution from the  $a$ -dependent function  $I_{00}$  must be cancelled by contributions computed numerically. The cancellation is more accurate for a larger exclusion zone but it is not possible to exceed the bounds of the singular cell therefore cancellation errors are minimised by putting  $2a$  equal to the smaller of  $\delta_y$  and  $\delta_z$ .

## VII. COMPARISON WITH EXPERIMENT

The boundary-element predictions have been compared with measurements made on narrow slots in aluminum alloys. The ideal crack theory assumes that the defect has a negligible opening and therefore it is important that the experiments are performed at a frequency such that the skin depth is large compared with the width of the slot. The parameters for two experiments are given in Table I, including, at the bottom of the list, the ratio of crack opening to skin depth. In both experiments the crack opening is less than 10% of the skin depth.

A comparison between predictions of the coil impedance change due to an ideal crack and experimental measurements is shown in Figs. 3 and 4. The measurements by Burke<sup>26</sup> are made at different coil positions with the coil axis in the plane of a rectangular slot. The coil starts at  $y=0$ , where the axis passes through the center of the slot. The calculations have been carried out using three different rectangular grids to give some indication of the stability of the results with respect to variations of the cell dimensions. The discrepancy between calculated and measured results for the  $32 \times 16$  grid is approximately 3%. Figure 4 compares the phase of the flaw signal with experiment showing that the predictions agree well with the measurements.

For the second comparison, the flaw profile was measured and the results of these measurements used to generate a set of coefficients to define the flaw shape in accordance

TABLE I. Probe and flaw parameters.

	Expt. 1	Expt. 2
Coil parameters		
inner radius ( $a_1$ )	$6.15 \pm 0.05$ mm	$2.51 \pm 0.01$ mm
outer radius ( $a_2$ )	$12.4 \pm 0.05$ mm	$7.38 \pm 0.01$ mm
length ( $2b$ )	$6.15 \pm 0.1$ mm	$4.99 \pm 0.01$ mm
lift-off ( $l$ )	0.88 mm	$0.30 \pm 0.01$ mm
number of turns	3790	4000
Frequency	900 Hz	417 Hz
Conductor		
conductivity	$30.6 \pm 0.02$ MS/m	$22.62 \pm 0.06$ MS/m
thickness	$12.22 \pm 0.02$ mm	24 mm
Flaw		
shape	rectangular	semielliptical
length ( $d$ )	$12.6 \pm 0.02$ mm	$22.1 \pm 0.05$ mm
depth ( $h$ )	$5.0 \pm 0.05$ mm	$8.61 \pm 0.05$ mm
opening ( $c$ )	$0.28 \pm 0.01$ mm	$0.33 \pm 0.01$ mm
Derived quantities		
skin depth ( $\delta$ )	$3.03 \pm 0.02$ mm	$5.18 \pm 0.01$ mm
opening/skin depth ( $c/\delta$ )	$0.092 \pm 0.003$	$0.063 \pm 0.002$

with Eq. (31). Although the slot is nominally semielliptical, there are slight departures from the nominal shape that are accounted for in the calculations. The predicted inductances due to an ideal crack are compared with the measurements in Fig. 5. The results show a very close agreement between the calculations and measurements, particularly for the  $32 \times 16$  cell lattice. The calculated resistance showed vary little change as the grid was varied (Fig. 6) but consistently underestimated the magnitude of the signal by a small amount.

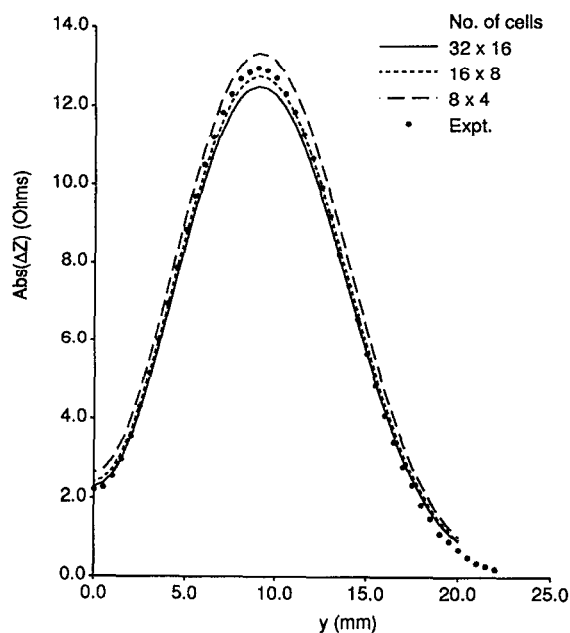


FIG. 3. Boundary-element predictions of the variation of absolute coil impedance due to a rectangular flaw compared with experiment at 900 Hz.

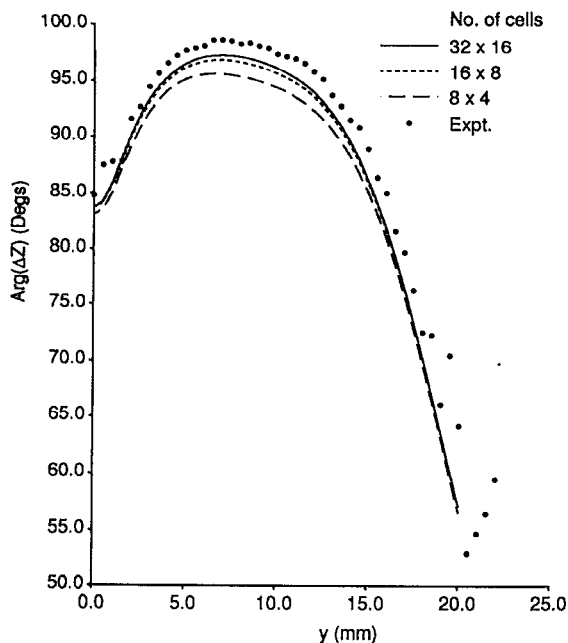


FIG. 4. Boundary-element predictions of the variation of the phase of the impedance change due to a rectangular flaw compared with experiment at 900 Hz.

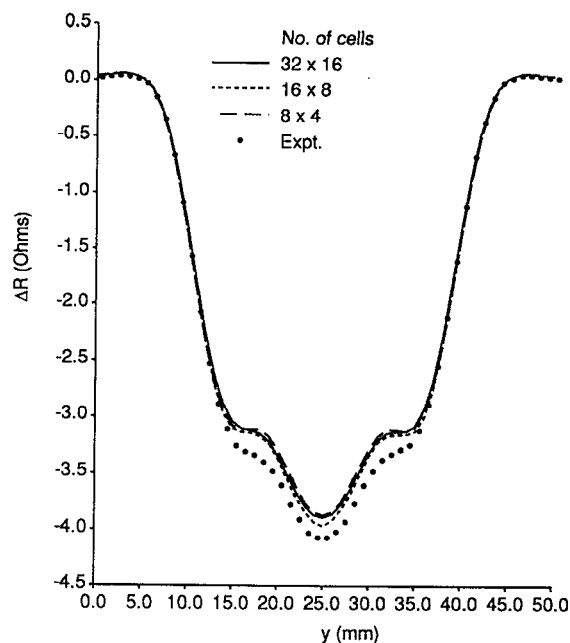


FIG. 6. Boundary-element predictions of the variation of coil resistance due to a flaw compared with experiment at 417 Hz.

## VIII. CONCLUSION

A theory has been developed for calculating the perturbed field due to an ideal crack in a half-space conductor. By representing the flaw in terms of an equivalent dipole density, a three-dimensional vector field problem has been reduced to one of finding a single component source distribution on a surface. The dipole density is given by a solution

of an integral equation with a singular kernel. The equation has been approximated using the moment method and a solution of the resulting matrix equation found by a LU decomposition.

A notable disadvantage of the moment method is that the accuracy of the results are difficult to predict and control. A piecewise constant solution is a crude approximation and one must be concerned about the errors this assumption introduces. On the other hand the predictions are often reasonably accurate even when only a few unknowns are used to define the dipole density on the crack. The calculation of, say, 50 impedances using a  $16 \times 8$  grid takes only about 20 s on a PC, including the calculation of the matrix. Although the speed of the calculation is not of major importance for making predictions, it is a significant factor in inversion where computational cost severely restricts what can be done. This issue is explored further in part II.

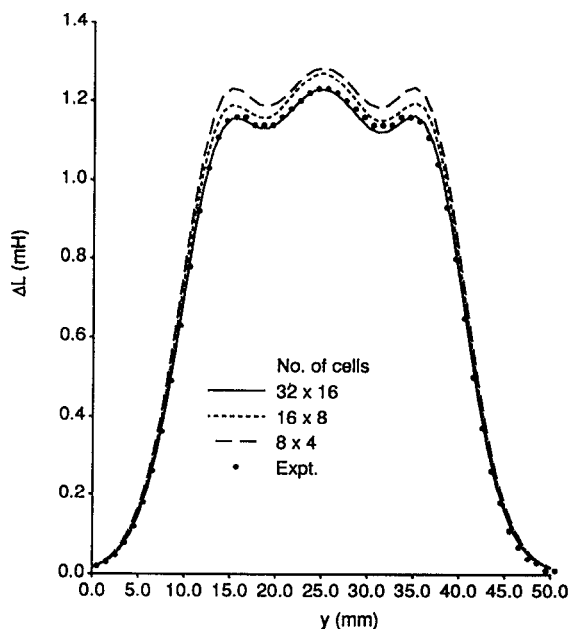


FIG. 5. Boundary-element predictions of the variation of coil self-inductance due to a flaw compared with experiment at 417 Hz.

## ACKNOWLEDGMENT

This work was supported by Defence Research Agency, Farnborough, and The Procurement Executive, MoD, U.K. The author would like to thank Dr. D. J. Harrison (DRA) for supplying experimental data on the semielliptical slot.

## APPENDIX: QUASISTATIC HALF-SPACE GREEN'S DYAD: TRANSVERSE ELECTRIC TERM

In this Appendix the transverse electric term from the half-space Green's dyad, Eq. (17), is expanded and expressed in terms of Kelvin functions. The term in question has the form

$$\frac{1}{k^2} \nabla \times \hat{z} \nabla' \times \hat{z} V(\mathbf{r}|\mathbf{r}') = \frac{1}{k^2} \begin{bmatrix} -\frac{\partial^2 V}{\partial y^2} & \frac{\partial^2 V}{\partial x \partial y} & 0 \\ \frac{\partial^2 V}{\partial x \partial y} & -\frac{\partial^2 V}{\partial x^2} & 0 \\ 0 & 0 & 0 \end{bmatrix}, \quad (\text{A1})$$

where  $V(\mathbf{r}|\mathbf{r}')$  is given by Eqs. (18)–(20). In order to get explicit expressions for the derivatives of  $V(\mathbf{r}|\mathbf{r}')$ , it is necessary to evaluate the derivatives of the function  $L$ . Rewriting Eq. (20), this function is given by

$$L = I_0(\alpha)K_0(\beta), \quad (\text{A2})$$

where  $\alpha = -ik(S - \zeta)/2$  and  $\beta = -ik(S + \zeta)/2$ . For the TE dyad we need  $L_{xxz}$ ,  $L_{yyz}$ , and  $L_{xyz}$ , the subscripts denoting derivatives. Taking the derivative with respect to  $z$  gives

$$L_z = [\alpha I_1(\alpha)K_0(\beta) + \beta I_0(\alpha)K_1(\beta)]/S, \quad (\text{A3})$$

hence

$$L_{xz} = -\frac{\alpha - \beta}{S} \frac{\partial \alpha}{\partial x} [I_1(\alpha)K_1(\beta) - I_0(\alpha)K_0(\beta)] - [\alpha I_1(\alpha)K_0(\beta) + \beta I_0(\alpha)K_1(\beta)] \frac{(\partial S/\partial x)}{S^2} \quad (\text{A4})$$

and

$$L_{xxz} = P_{00}I_0(\alpha)K_0(\beta) + P_{01}I_0(\alpha)K_1(\beta) + P_{10}I_1(\alpha)K_0(\beta) + P_{11}I_1(\alpha)K_1(\beta), \quad (\text{A5})$$

where

$$P_{00} = -\frac{\partial}{\partial x} \left( \frac{\alpha - \beta}{S} \frac{\partial \alpha}{\partial x} \right) + \left( \frac{\alpha - \beta}{S^2} \right) \left( \frac{\partial \alpha}{\partial x} \right) \left( \frac{\partial S}{\partial x} \right), \quad (\text{A6})$$

$$P_{01} = \frac{1}{S^2} \frac{\partial \alpha}{\partial x} \left( \frac{\partial S}{\partial x} \right) - \frac{\partial}{\partial x} \left( \frac{\beta}{S^2} \frac{\partial S}{\partial x} \right) - 2 \left( \frac{\alpha - \beta}{S} \right) \left( \frac{\partial \alpha}{\partial x} \right)^2, \quad (\text{A7})$$

$$P_{10} = \frac{1}{S^2} \frac{\partial \alpha}{\partial x} \left( \frac{\partial S}{\partial x} \right) - \frac{\partial}{\partial x} \left( \frac{\alpha}{S^2} \frac{\partial S}{\partial x} \right) + 2 \left( \frac{\alpha - \beta}{S} \right) \left( \frac{\partial \alpha}{\partial x} \right)^2, \quad (\text{A8})$$

and

$$P_{11} = \left( \frac{\alpha - \beta}{S^2} \right) \left( \frac{\partial \alpha}{\partial x} \right) \frac{\partial S}{\partial x} - \frac{\partial}{\partial x} \left( \frac{\alpha - \beta}{S} \frac{\partial \alpha}{\partial x} \right) + \left( \frac{1}{\alpha} + \frac{1}{\beta} \right) \times \left( \frac{\alpha - \beta}{S} \right) \left( \frac{\partial \alpha}{\partial x} \right)^2. \quad (\text{A9})$$

Differentiating with respect to  $x$  in Eqs. (A6)–(A9) gives

$$P_{00} = \frac{k^2 \zeta}{2S^2} \left[ 1 - 3 \left( \frac{x - x'}{S} \right)^2 \right], \quad (\text{A10})$$

$$P_{01} = \frac{ik}{2S^2} \left\{ \left( \frac{S + \zeta}{S} \right) \left[ 1 - 3 \left( \frac{x - x'}{S} \right)^2 \right] + k^2 \zeta S \left( \frac{x - x'}{S} \right)^2 \right\}, \quad (\text{A11})$$

$$P_{10} = \frac{ik}{2S^2} \left\{ \left( \frac{S - \zeta}{S} \right) \left[ 1 - 3 \left( \frac{x - x'}{S} \right)^2 \right] - k^2 \zeta S \left( \frac{x - x'}{S} \right)^2 \right\}, \quad (\text{A12})$$

and

$$P_{11} = -\frac{k^2 \zeta}{2S^2} \left[ 1 - 3 \left( \frac{x - x'}{S} \right)^2 - 2 \frac{(x - x')^2}{(S^2 - \zeta^2)} \right]. \quad (\text{A13})$$

The expression for  $L_{yyz}$  has the same form as Eq. (A5) with  $y - y'$  replacing  $x - x'$  in Eqs. (A10)–(A13). Similarly  $L_{xyz}$  can be written as

$$L_{xyz} = Q_{00}I_0(\alpha)K_0(\beta) + Q_{01}I_0(\alpha)K_1(\beta) + Q_{10}I_1(\alpha)K_0(\beta) + Q_{11}I_1(\alpha)K_1(\beta), \quad (\text{A14})$$

where

$$Q_{00} = \frac{\partial}{\partial y} \left( \frac{\alpha - \beta}{S} \frac{\partial \alpha}{\partial x} \right) - \left( \frac{\alpha - \beta}{S^2} \right) \left( \frac{\partial \alpha}{\partial x} \right) \left( \frac{\partial S}{\partial y} \right), \quad (\text{A15})$$

$$Q_{01} = \frac{1}{S^2} \frac{\partial \alpha}{\partial y} \left( \frac{\partial S}{\partial x} \right) - \frac{\partial}{\partial y} \left( \frac{\beta}{S^2} \frac{\partial S}{\partial x} \right) - 2 \left( \frac{\alpha - \beta}{S} \right) \left( \frac{\partial \alpha}{\partial x} \right) \left( \frac{\partial \alpha}{\partial y} \right), \quad (\text{A16})$$

$$Q_{10} = \frac{1}{S^2} \frac{\partial \alpha}{\partial y} \left( \frac{\partial S}{\partial x} \right) - \frac{\partial}{\partial y} \left( \frac{\alpha}{S^2} \frac{\partial S}{\partial x} \right) + 2 \left( \frac{\alpha - \beta}{S} \right) \left( \frac{\partial \alpha}{\partial x} \right) \left( \frac{\partial \alpha}{\partial y} \right), \quad (\text{A17})$$

and

$$Q_{11} = \left( \frac{\alpha - \beta}{S^2} \right) \left( \frac{\partial \alpha}{\partial y} \right) \frac{\partial S}{\partial x} - \frac{\partial}{\partial y} \left( \frac{\alpha - \beta}{S} \frac{\partial \alpha}{\partial x} \right) + \left( \frac{1}{\alpha} + \frac{1}{\beta} \right) \left( \frac{\alpha - \beta}{S} \right) \left( \frac{\partial \alpha}{\partial x} \right) \left( \frac{\partial \alpha}{\partial y} \right). \quad (\text{A18})$$

Carrying out the differentiation in Eqs. (A15)–(A18) gives

$$Q_{00} = -\frac{3k^2 \zeta}{2S^4} (x - x')(y - y'), \quad (\text{A19})$$

$$Q_{01} = -\frac{ik}{2S^4} \left[ 3 \left( \frac{S + \zeta}{S} \right) - k^2 \zeta S \right] (x - x')(y - y'), \quad (\text{A20})$$

$$Q_{10} = -\frac{ik}{2S^4} \left[ 3 \left( \frac{S - \zeta}{S} \right) + k^2 \zeta S \right] (x - x')(y - y'), \quad (\text{A21})$$

and

$$Q_{11} = \frac{k^2 \zeta}{2S^2} \left( \frac{3}{S^2} + \frac{2}{S^2 - \zeta^2} \right) (x - x')(y - y'). \quad (\text{A22})$$

Finally, the modified Bessel functions with complex arguments are expressed in terms of Kelvin functions as follows:<sup>21</sup>

$$I_0(\alpha) = \text{ber}(\xi) - i \text{bei}(\xi) \quad (\text{A23})$$

$$I_1(\alpha) = \frac{1}{\sqrt{2}} [(1 + i)\text{ber}'(\xi) + (1 - i)\text{bei}'(\xi)], \quad (\text{A24})$$

$$K_0(\beta) = \text{ker}(\eta) - i \text{kei}(\eta), \quad (\text{A25})$$

$$K_1(\beta) = -\frac{1}{\sqrt{2}} [(1 + i)\text{ker}'(\eta) + (1 - i)\text{kei}'(\eta)], \quad (\text{A26})$$

where  $\xi = \sqrt{2} \text{Re}(\alpha)$  and  $\eta = \sqrt{2} \text{Re}(\beta)$ .

- <sup>1</sup>J. R. Bowler, S. A. Jenkins, L. D. Sabbagh, and H. A. Sabbagh, *J. Appl. Phys.* **70**, 1107 (1991).
- <sup>2</sup>D. McA. McKirdy, *J. Nondestruct. Eval.* **8**, 45 (1989).
- <sup>3</sup>R. E. Beissner, *J. Appl. Phys.* **60**, 352 (1986).
- <sup>4</sup>A. P. Raiche and J. H. Coggon, *Geophys. J. R. Astron. Soc.* **42**, 1035 (1975).
- <sup>5</sup>C.-T. Tai, *Dyadic Green's Functions in Electromagnetic Theory* (Intex, Scranton, 1971).
- <sup>6</sup>P. E. Wannamaker, G. W. Hohmann, and W. A. SanFilipo, *Geophysics* **49**, 60 (1984).
- <sup>7</sup>M. L. Burrows, Ph.D. thesis, University of Michigan, Ann Arbor, Michigan, 1964.
- <sup>8</sup>R. F. Harrington, *Field Computation by Moment Methods* (Macmillan, New York, 1968).
- <sup>9</sup>A. H. Kahn, R. Spal, and A. Feldman, *J. Appl. Phys.* **48**, 4454 (1977).
- <sup>10</sup>A. Sommerfeld, *Optics* (Academic, New York, 1964).
- <sup>11</sup>S. K. Burke and L. R. F. Rose, *Proc. R. Soc. London Ser. A* **418**, 229 (1988).
- <sup>12</sup>J. R. Bowler, in *Review of Progress in Quantitative Nondestructive Evaluation* (Plenum, New York, 1990), Vol. 5A, p. 149.
- <sup>13</sup>R. Plonsey and R. E. Collins, *Principles and Applications of Electromagnetic Fields* (McGraw-Hill, New York, 1961), p. 236.
- <sup>14</sup>J. A. Stratton, *Electromagnetic Theory* (McGraw-Hill, New York, 1941), pp. 34–36.
- <sup>15</sup>J. A. Stratton, *Electromagnetic Theory* (McGraw-Hill, New York, 1941), p. 191.
- <sup>16</sup>J. Hadamard, *Lectures on Cauchy's Problem in Linear partial Differential Equations* (Dover, New York, 1952).
- <sup>17</sup>M. J. Lighthill, *Fourier Analysis and Generalized Functions* (Cambridge University Press, Cambridge, 1962).
- <sup>18</sup>A. Banos, *Dipole Radiation in the Presence of a Conducting Half-Space* (Pergamon, Oxford, 1966), p. 135.
- <sup>19</sup>J. R. Bowler, *J. Appl. Phys.* **61**, 839 (1987).
- <sup>20</sup>I. S. Gradshteyn and I. M. Ryzhik, *Tables of Integrals, Series and Products* (Academic, New York, 1980), Table, 6.637, p. 719.
- <sup>21</sup>M. Abramowitz and I. A. Stegun, *Handbook of Mathematical Functions with Formulas, Graphs, and Mathematical Tables* (Wiley, New York, 1972), Chap. 9.
- <sup>22</sup>R. F. Harrington, *Time Harmonic Electromagnetic Fields* (McGraw-Hill, New York, 1961).
- <sup>23</sup>I. S. Gradshteyn and I. M. Ryzhik, *Tables of Integrals, Series and Products* (Academic, New York, 1980), Table 6.561, p. 683.
- <sup>24</sup>W. A. Davis and R. Mittra, *IEEE Trans. Antennas Prop.* **AP-25**, 402 (1977).
- <sup>25</sup>D. B. Miron, *IEEE Trans. Antennas Prop.* **AP-31**, 507 (1983).
- <sup>26</sup>S. K. Burke, *J. Nondestruct. Eval.* **7**, 35 (1988).